J. Fluid Mech. (1982), *vol.* 124, *pp.* 27–43
Printed in Great Britain

Gravitational and zero-drag motion of a sphere of arbitrary size in an inclined channel at low Reynolds number

By PETER GANATOS, SHELDON WEINBAUM AND ROBERT PFEFFER

The City College of The City University of New York, New York, NY 10031

(Received 5 January 1982 and in revised form 17 May 1982)

The strong-interaction theory developed in Ganatos, Weinbaum & Pfeffer (1980*a*) and Ganatos, Pfeffer & Weinbaum (1980*b*) for the normal and parallel creeping motion of a sphere of arbitrary size between two infinite plane-parallel walls is applied to several particle–boundary interaction problems of long-standing interest. The first highly accurate solutions are presented for the slip and angular velocity of a neutrally buoyant sphere carried by the fluid in a Couette or Poiseuille channel flow and the gravitational settling of a non-neutrally buoyant sphere in an inclined channel. The latter problem clearly illustrates the non-isotropy of the frictional resistance tensor on the particle motion. The solutions for the fluid velocity field exhibit an induced circulation extending to infinity fore and aft of the sphere for a neutrally buoyant sphere in Couette flow and an induced back-flow ahead of the sphere for the Poiseuille flow geometry. Approximate but highly accurate solutions are presented for small gap widths between a sphere and the neighbouring boundary, which take account of the influence of the second wall.

1. Introduction

In two recent papers the authors have shown that it is possible to extend the three-dimensional boundary collocation solution technique first introduced by Ganatos, Pfeffer & Weinbaum (1978) for strongly interacting spheres in unbounded flow at low Reynolds number to simple bounded-flow problems and have obtained analytical–numerical solutions for a sphere of arbitrary size moving between infinite parallel boundaries. In the first paper (Ganatos, Weinbaum & Pfeffer 1980*a*) solutions were obtained for the force on a sphere translating perpendicular to the confining walls. In the second paper (Ganatos, Pfeffer & Weinbaum 1980*b*) solutions are presented for the force and torque on a sphere that is translating parallel to the walls, rotating about an axis parallel to the walls, or which is held rigidly in place in a two-dimensional Poiseuille or simple shear flow. The important features of these solutions are that the no-slip boundary conditions on the confining walls are satisfied by exact analytic methods for a sphere of arbitrary size and position and the boundary conditions on the surface of the sphere are satisfied to any order of accuracy using a truncated boundary collocation series of fundamental solutions for the spherical disturbance. In this manner, one is able to obtain the first three-dimensional strong-interaction solutions for a particle with closely spaced confining walls in the creeping-motion regime.

In the present paper, the results for the force and torque coefficients presented in

Ganatos *et al.* (1980*a*, *b*) are used to obtain solutions for several flow problems of long-standing interest. These include the local translational and rotational velocities of a neutrally buoyant sphere in zero-drag motion in a Couette or Poiseuille channel flow and the gravitational settling of a non-neutrally buoyant sphere in an inclined channel. The zero-drag motions are of interest in a variety of two-phase-flow applications where dispersed small particles are carried along by the fluid, e.g. a contaminant particle in a lubricating bearing. Biological applications include the flow of the cellular components of blood in the microvasculature and osmotic phenomena associated with the reflection of solute molecules passing through the small extracellular channels between adjacent cells in a cell layer. Prior to the present analysis, much of the existing theoretical modelling had been based on the widely used weak-interaction method-of-reflection technique. Highly accurate approximate lubrication-type solutions are also presented herein for small gap widths (less than a tenth of a sphere radius), which take account of the influence of the more-distant boundary.

For more than a decade, boundary collocation methods have been used for treating the zero-Reynolds-number strong interaction between closely spaced spheres and spheroids or between spheres and confining walls. By analytically exact we mean that each of the terms in the solution is an exact solution of the governing differential equation and that the infinite summation of terms representing each spheroid converges to its exact description. All the early studies were confined to periodic or infinite-domain bounded and unbounded flows where the existence of an axisymmetric stream function permitted a relatively simple description of the velocity field and no direct treatment of the Navier–Stokes equation for the pressure was required. Some of the more important of the early papers include the flow past coaxial clusters of spheroids (Gluckman, Pfeffer & Weinbaum 1971), motion of an infinite periodic array of spheres along the axis of a circular cylinder (Wang & Skalak 1969), and the arbitrary axial motion of two or more spheres in an infinite tube of circular cross-section (Leichtberg, Pfeffer & Weinbaum 1976). The extension of this analysis to multiple-domain problems, such as the flow through a finite-length circular pore or a sphere approaching an orifice along its centreline, does require an explicit treatment of the pressure field in the matching of the stress tensor at the interface between regions and is described in Dagan, Weinbaum & Pfeffer (1982*a*, *b*). Exact three-dimensional boundary collocation techniques require a different approach, which is described in detail in Ganatos *et al.* (1978, 1980*a*, *b*). We shall give a very brief summary of this solution procedure here in the context of the particular flow configurations to be studied in the present paper.

The velocity disturbance produced by each particle or boundary in the flow field is represented by an infinite series or Fourier integral of all the simply separable solutions of the Stokes-flow governing equations in the appropriate coordinate system. For three-dimensional flows these fundamental solutions are obtained by first writing a general solution of Laplace's equation for the pressure field and then solving the Navier–Stokes and continuity equations for the three velocity components in terms of the pressure using three scalar or vector potential functions. For a spherical boundary these fundamental solutions are simply Lamb's spherical harmonic functions. Because of the linearity of the governing equations and boundary conditions, the total solution for the velocity field is a superposition of the fundamental solutions for all spheres and confining boundaries. The no-slip boundary conditions are first satisfied on the confining boundaries of infinite extent. This step must be performed analytically since collocation procedures cannot easily be applied to such boundaries.

For planar boundaries, as in the present application, this step involves rewriting the spherical disturbances in terms of rectangular coordinates and then performing analytically a double Fourier inversion of the spherical disturbances that are felt on the confining boundaries. This procedure leads to closed-form expressions for the Fourier spectral functions describing the wall disturbance in terms of the unknown constants in the spherical-harmonic series. In this manner, the total solution for the velocity field is reduced to an infinite series for each velocity component containing three sets of unknown coefficients, which exactly satisfies the no-slip boundary conditions on all the confining walls independently of the value of the spherical harmonic coefficients. These coefficients are determined by a collocation procedure in which the infinite series are truncated and the three no-slip boundary conditions are satisfied at discrete points on the surface of each sphere. Because the fundamental separable solutions for each particle and boundary in the appropriate coordinate system provide a good description of the disturbance produced by that body and because the method satisfies the no-slip boundary conditions on all the particles and boundaries simultaneously rather than in an iterative fashion, as in the method of reflections, the method converges quickly to the exact solution as the number of collocation points is increased.

The accuracy of the converged collocation solutions have been tested in Ganatos *et al.* (1980*a*, *b*) by detailed comparison with the exact bipolar coordinate solutions of Brenner (1961) for the motion of a sphere perpendicular to a single plane wall and Goldman, Cox & Brenner (1967*a*, *b*) for the drag and torque on a sphere translating parallel to the wall, rotating adjacent to the wall, or in the presence of a shear field. In all cases the converged collocation solutions for the force and torque coefficients were in perfect agreement with the exact solutions for all spacings tested down to a gap width of a tenth of a radius. On the other hand, it was found that the first-order reflection theory of Ho & Leal (1974) provides reasonable agreement with the collocation results for the drag only when the sphere is five or more radii from both walls. At closer spacings first-order reflection theory was found to be highly inaccurate. For example, the drag on a sphere translating midway between two walls in a direction perpendicular to the walls is 40 % below the true value when the walls are spaced two sphere diameters apart and one order-of-magnitude lower at a spacing of 1·1 diameters. The first-order reflection theory also predicts an erroneous direction for the torque on a sphere translating parallel to the walls for certain particle positions. Comparison with the classical higher-order method-of-reflection solutions of Faxen (1923) also showed that the convergence of the multiple-reflection series solutions is poor when the sphere centre is less than two radii from either boundary.

In the present work, strong-interaction solutions are presented for the gravitational and zero-drag motion of a sphere in an inclined channel. The paper is presented in four sections. Section 2 contains solutions for the general motion of a sphere between two walls, including approximate solutions for small fluid gap widths. In §3 solutions are presented for the trajectory of a sphere settling under gravity in an inclined channel. Finally, §4 contains solutions for the zero-drag motion of a sphere in two-dimensional Poiseuille flow or Couette flow in a channel.

2. General motion of a sphere in a channel

Consider the motion of a sphere of radius a in a viscous fluid between two plane-parallel walls spaced at a distance of b and c from the sphere centre, as shown in figure 1. The sphere is translating in an arbitrary direction with velocity $\mathbf{U}$, which

has components U_x and U_z, and rotating with angular velocity $\boldsymbol{\Omega}$, which has only one component Ω_y. A unidirectional incident flow $V_\infty(z)$ may be present in the x-direction owing to an imposed pressure gradient or to the motion of the upper wall.

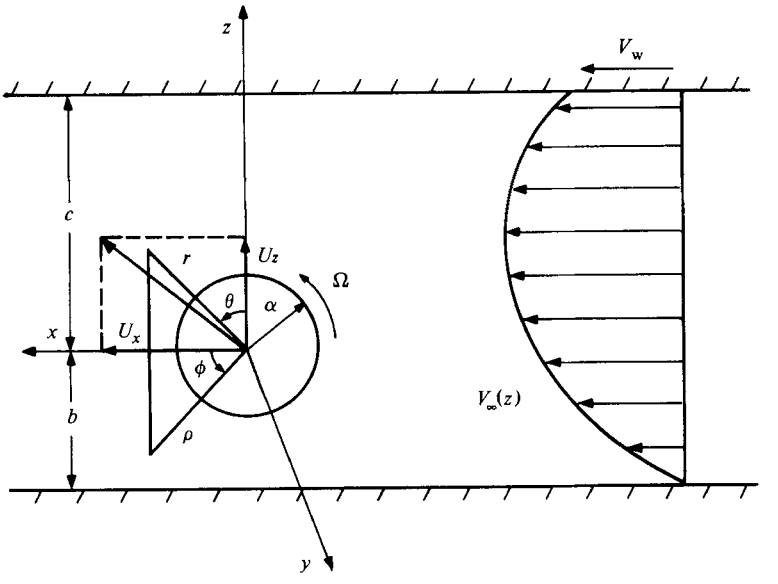

FIGURE 1. Geometry of the general flow configuration.

In the low-Reynolds-number flow limit, the fluid velocity $\mathbf{V}$ must satisfy the creeping-flow equations

$$\mu\nabla^2\mathbf{V} = \nabla p, \quad \nabla.\mathbf{V} = 0, \tag{2.1a, b}$$

subject to the boundary conditions

$$\mathbf{V} = \mathbf{U} + \boldsymbol{\Omega}\times a\hat{\mathbf{e}}_r \quad \text{on} \quad r = a, \tag{2.2a}$$

$$\mathbf{V} = \mathbf{V}_\infty \quad \text{on} \quad z = -b, c \quad \text{or} \quad x \to \pm\infty, \tag{2.2b}$$

where the incident flow field $\mathbf{V}_\infty$ is given by

$$\mathbf{V}_\infty(z) = \left[S(z+b) - \frac{V_c(z+b)(z-c)}{4(b+c)^2}\right]\hat{\mathbf{i}}. \tag{2.3}$$

The first term in (2.3) represents pure Couette flow induced by the motion of the upper wall, where the shear rate is $S = V_w/(b+c)$ (see figure 1). The second term represents pure Poiseuille flow, where V_c is the undisturbed centreline velocity if the walls are stationary.

Because of the linearity of the governing equations and boundary conditions, the velocity field $\mathbf{V}$ for the general problem posed by (2.1)–(2.3) may be decomposed into five parts:

$$\mathbf{V} = \mathbf{V}^{\mathrm{t}}_x + \mathbf{V}^{\mathrm{t}}_z + \mathbf{V}^{\mathrm{r}}_y + \mathbf{V}^{\mathrm{s}}_x + \mathbf{V}^{\mathrm{p}}_x, \tag{2.4}$$

where each contribution satisfies the creeping-motion equations (2.1). The contribution $\mathbf{V}^{\mathrm{t}}_x$ represents the velocity field due to translation of a sphere with velocity U_x parallel to the walls with no rotation in an otherwise quiescent fluid. $\mathbf{V}^{\mathrm{t}}_z$ represents the axisymmetric fluid motion induced by a pure translation of the sphere with velocity U_z perpendicular to the walls. $\mathbf{V}^{\mathrm{r}}_y$ is the fluid motion produced by a sphere

rotating with angular velocity Ω_y about an axis parallel to the walls in a quiescent fluid at infinity. The contributions $\mathbf{V}_x^{\mathrm{s}}$ and $\mathbf{V}_x^{\mathrm{p}}$ represent Couette and Poiseuille flow respectively past a rigidly held sphere between the two walls.

The force and torque acting on the particle resulting from the motions described by (2.4) may be expressed using nine non-zero resistance coefficients as follows:

$$F_x = 6\pi\mu a[U_x F_x^{\mathrm{t}} + a\Omega F_x^{\mathrm{r}} + V_{\mathrm{c}} F_x^{\mathrm{p}} + bSF_x^{\mathrm{s}}], \tag{2.5}$$

$$F_z = 6\pi\mu a U_z F_z^{\mathrm{t}}, \tag{2.6}$$

$$T_y = 8\pi\mu a^2[U_x T_y^{\mathrm{t}} + a\Omega T_y^{\mathrm{r}} + V_c T_y^{\mathrm{p}} + \tfrac{1}{2}aST_y^{\mathrm{s}}]. \tag{2.7}$$

Here the pairs $(F_x^{\mathrm{t}}, T_y^{\mathrm{t}})$, $(F_z^{\mathrm{t}}, 0)$, $(F_x^{\mathrm{r}}, T_y^{\mathrm{r}})$, $(F_x^{\mathrm{s}}, T_y^{\mathrm{s}})$ and $(F_x^{\mathrm{p}}, T_y^{\mathrm{p}})$ are the force and torque coefficients corresponding to the motions $\mathbf{V}_x^{\mathrm{t}}$, $\mathbf{V}_z^{\mathrm{t}}$, $\mathbf{V}_y^{\mathrm{r}}$, $\mathbf{V}_x^{\mathrm{s}}$ and $\mathbf{V}_x^{\mathrm{p}}$ respectively. The torque coefficient corresponding to $\mathbf{V}_z^{\mathrm{t}}$ is zero since this fluid motion is axisymmetric. The nine resistance coefficients account for wall effects on the particle and depend on the ratio $\alpha = d/2a$ of channel width to particle size and on the particle position $s = b/d$, where $d = b+c$ (see figure 1). Numerical values of F_z^{t} have been computed to a high degree of accuracy using the boundary collocation series solution technique, and are given in Ganatos *et al.* (1980*a*) and Ganatos (1979). Values of the remaining eight coefficients computed by the same technique are given in Ganatos *et al.* (1980*b*) and Ganatos (1979).

If the particle is free to rotate about the y-axis, the net torque on the particle is zero. Solving (2.7) for the angular velocity Ω and substituting into (2.5), one can rewrite (2.5) in the form

$$F_x = -\frac{6\pi\mu a}{F(\alpha, s)}[U_x - G(\alpha, s)\, V_{\mathrm{c}} - H(\alpha, s)\, V_{\mathrm{w}}], \tag{2.8}$$

where

$$F(\alpha, s) = \frac{-T_y^{\mathrm{r}}}{F_x^{\mathrm{t}} T_y^{\mathrm{r}} - F_x^{\mathrm{r}} T_y^{\mathrm{t}}}, \tag{2.9}$$

$$G(\alpha, s) = \frac{F_x^{\mathrm{r}} T_y^{\mathrm{p}} - F_x^{\mathrm{p}} T_y^{\mathrm{r}}}{F_x^{\mathrm{t}} T_y^{\mathrm{r}} - F_x^{\mathrm{r}} T_y^{\mathrm{t}}}, \tag{2.10}$$

$$H(\alpha, s) = \frac{(1/4\alpha)\, F_x^{\mathrm{r}} T_y^{\mathrm{s}} - sF_x^{\mathrm{s}} T_y^{\mathrm{r}}}{F_x^{\mathrm{t}} T_y^{\mathrm{r}} - F_x^{\mathrm{r}} T_y^{\mathrm{t}}}. \tag{2.11}$$

The F, G and H function may be computed using (2.9), (2.10) and (2.11) with values of the force and torque coefficients contained in Ganatos *et al.* (1980*b*) for $b/a \geqslant 1{\cdot}1$. At closer particle-to-wall spacings the boundary collocation truncated series solution technique used to compute these coefficients becomes too time-consuming since more than 20 boundary points are required for an accuracy of 0·1 % on some of the force and torque coefficients. A more expedient approach is to use an analytic approximation in which the exact bipolar solutions in the range $1{\cdot}0032 \leqslant b/a \leqslant 1{\cdot}1$ and lubrication formulas for $b/a \leqslant 1{\cdot}0032$ of Goldman *et al.* (1967*a*, *b*) and Cox & Brenner (1967) for the various force and torque coefficients describing the motion of a sphere near a single plane wall are modified by adding a function of α to account for the nearly constant effects of the more-distant boundary. Thus in the presence of two walls

$$\left.\begin{aligned} F_x^{\mathrm{t}} &= (F_x^{\mathrm{t}})_{\text{one wall}} + A(\alpha), \\ T_y^{\mathrm{t}} &= (T_y^{\mathrm{t}})_{\text{one wall}} + B(\alpha), \\ &\vdots \qquad\quad \vdots \qquad\quad \vdots \end{aligned}\right\} \quad b/a \leqslant 1{\cdot}1, \tag{2.12}$$

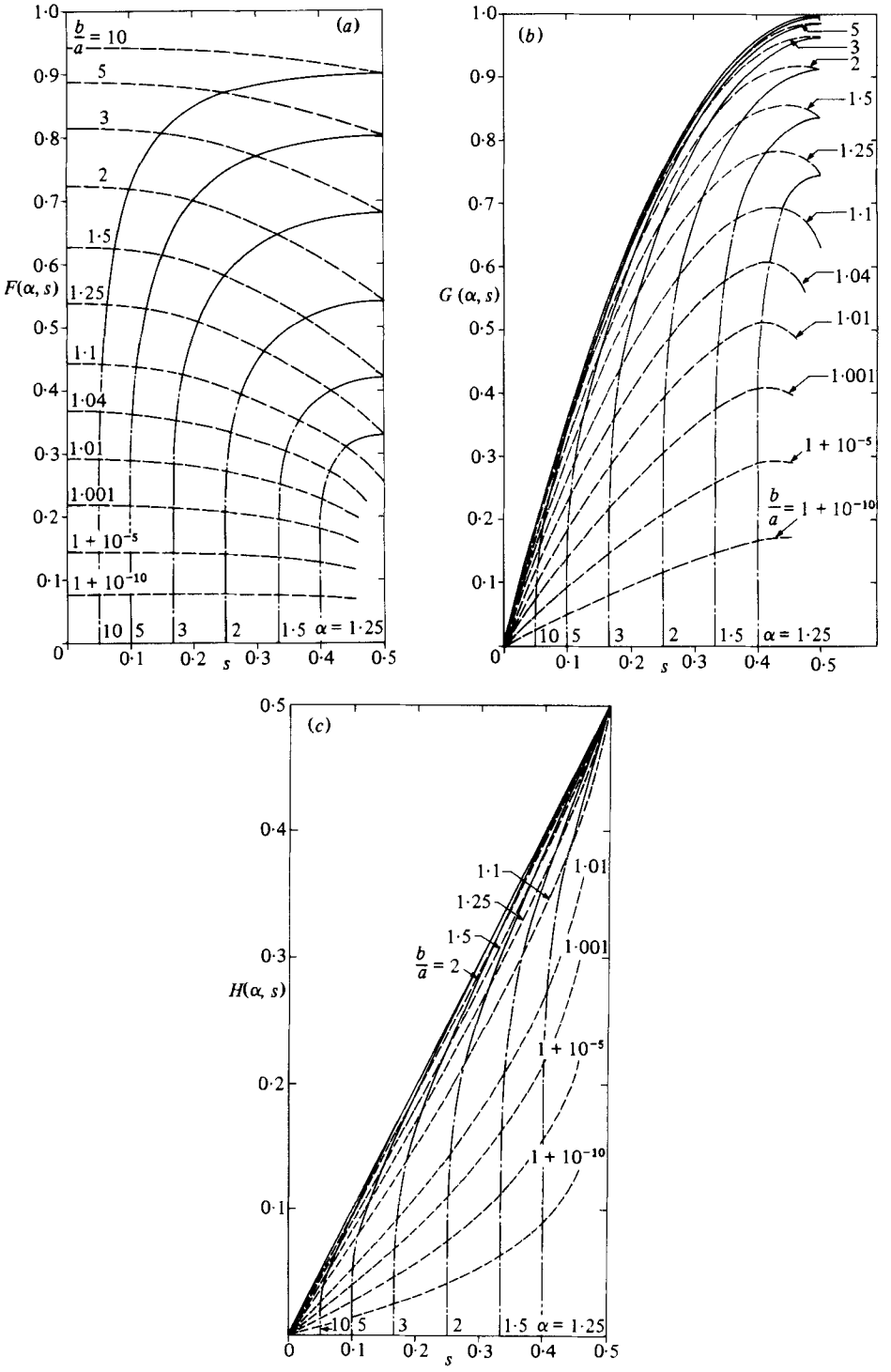

FIGURE 2. Variation of (*a*) F, (*b*) G and (*c*) H drag functions with channel width α and particle position s: ——, collocation theory for α = const; — — — —, lubrication theory for α = const; - - - - - - -, b/a = const.

where the functions on the right-hand side of (2·12) are constant for any given channel width. These functions are evaluated by matching the lubrication formulas (2.12) with the two-wall collocation solutions for the respective force and torque coefficients at $b/a = 1{\cdot}1$ that are given in Ganatos *et al.* (1980*a*, *b*). Thus

$$\left.\begin{aligned} A(\alpha) &= (F_x^{\mathrm{t}})_{1\cdot1} - (F_{x\ \mathrm{one\ wall}}^{t})_{1\cdot1}, \\ B(\alpha) &= (T_y^{\mathrm{t}})_{1\cdot1} - (T_{y\ \mathrm{one\ wall}}^{\mathrm{t}})_{1\cdot1}, \\ &\vdots \qquad\quad \vdots \qquad\quad \vdots \end{aligned}\right\} \tag{2.13}$$

where the subscript 1·1 indicates that the quantity has been evaluated at $b/a = 1{\cdot}1$.

Unfortunately, a similar procedure cannot be used to determine the limiting behaviour of F_x^{p} and T_y^{p} as $b/a \to 1$ because these coefficients are undefined for flow bounded by a single plane. However, these coefficients converge to finite values as $b/a \to 1$ and their converged value deviates very little from their value at $b/a = 1{\cdot}1$. Thus approximate values of these coefficients were obtained by a linear extrapolation of the results presented in Ganatos *et al.* (1980*b*) to $b/a = 1$. The extrapolated data is believed to be accurate to about 0·1 %.

The variation of F, G and H with particle position is shown in figure 2. The curves in the range $b/a \geqslant 1{\cdot}1$ were obtained using the collocation theory of Ganatos *et al.* (1980*a*, *b*). The solid lines show the variation of these functions with particle position s at various fixed channel widths α. The dashed lines show the effect of the position of the wall at $z = c$ for various sphere-to-wall spacings b/a. The broken lines for $b/a < 1{\cdot}1$ are the lubrication-theory results obtained from (2.12) and (2.13) for constant α. Evidence of the high accuracy of the lubrication theory is found in the continuity of the slope at $b/a = 1{\cdot}1$ where the two solutions are matched.

In computing the lubrication limits for the F, G and H functions, it was found that the analytic lubrication formulas given by Goldman *et al.* (1967*a*, *b*) for the various force and torque coefficients describing the motion of a sphere near a single plane wall, which are strictly valid only in the range $b/a \leqslant 1{\cdot}0032$, could be used in (2.12) and (2.13) to represent the one-wall force and torque coefficients in the entire range $1 \leqslant b/a \leqslant 1{\cdot}1$. For example, using this approximation in (2.9) and neglecting higher-order terms yields the simple formula

$$\frac{1}{F} = -\tfrac{1}{2}\ln\left(\frac{b}{a} - 1\right) + C(\alpha) \quad \left(\frac{b}{a} \leqslant 1{\cdot}1\right), \tag{2.14}$$

where the function $C(\alpha)$ is evaluated by matching (2.14) with the value of F computed from the two-wall collocation solutions at $b/a = 1{\cdot}1$ given in Ganatos *et al.* (1980*a*, *b*). Results obtained by this formula were found to be virtually indistinguishable from those obtained from (2.12) and (2.13). On the other hand, the angular velocity of the particle, computed using a similar approximation, showed a discontinuity in slope at $b/a = 1{\cdot}1$. Thus the more-accurate formulas (2.12) and (2.13) were used to compute all of the lubrication solutions presented in this paper.

We next examine special applications of (2.8) that are of practical interest and importance, namely the gravitational settling motion and zero-drag motion of a sphere in a channel.

3. Sphere settling under gravity in an inclined channel

In this section, solutions are presented for the motion of a sphere settling under gravity, in a channel inclined at an angle β with quiescent fluid at infinity. The configuration is shown in figure 3, where the sphere is released from the position $x = 0$,

$z = z_0$. A force and torque balance on the particle using (2.5)–(2.7) yields

$$6\pi\mu a[U_x F_x^{\mathrm{t}} + a\Omega F_x^{\mathrm{r}}] + \tfrac{4}{3}\pi a^3(\rho_{\mathrm{s}} - \rho) g \sin\beta = 0, \tag{3.1}$$

$$6\pi\mu a U_z F_z^{\mathrm{t}} + \tfrac{4}{3}\pi a^3(\rho_{\mathrm{s}} - \rho) g \cos\beta = 0, \tag{3.2}$$

$$8\pi\mu a^2[U_x T_y^{\mathrm{t}} + a\Omega T_y^{\mathrm{r}}] = 0. \tag{3.3}$$

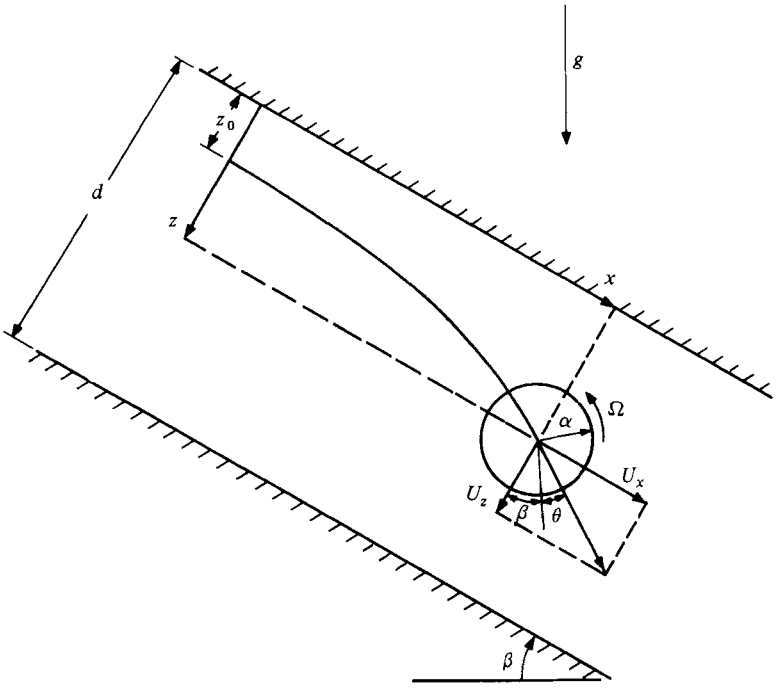

FIGURE 3. Schematic diagram of a sphere settling under gravity in an inclined channel.

The solution of (3.1)–(3.3) is conveniently written in terms of the dimensionless velocity ratios

$$\frac{U_x}{U_{\mathrm{t}}} = F \sin\beta, \tag{3.4}$$

$$\frac{U_z}{U_{\mathrm{t}}} = \frac{-\cos\beta}{F_z^{\mathrm{t}}}, \tag{3.5}$$

$$\frac{a\Omega}{U_{\mathrm{t}}} = \frac{-T_y^{\mathrm{t}}}{T_y^{\mathrm{r}}} F \sin\beta, \tag{3.6}$$

where $U_{\mathrm{t}} = (2a^2/9\mu)\,(\rho_{\mathrm{s}} - \rho)\, g$ is the terminal settling velocity of an isolated sphere in an unbounded medium, and F is given by (2.9) (see figure 2a).

From (3.4) and (3.5) the trajectory of the settling sphere is given by

$$\frac{dx}{dz} = \frac{U_x}{U_z} = -F_z^{\mathrm{t}} F \tan\beta = \frac{\tan\beta}{f(\alpha, z)}, \tag{3.7}$$

where the function $f(\alpha, z)$ is plotted in figure 4 for various channel widths α. The figure also shows that for a fixed distance between the sphere and the closer wall (z/a = const) the function $f(\alpha, z)$ is relatively insensitive to the position of the second wall.

Figure 5 shows a representative solution for the trajectory of a sphere released at

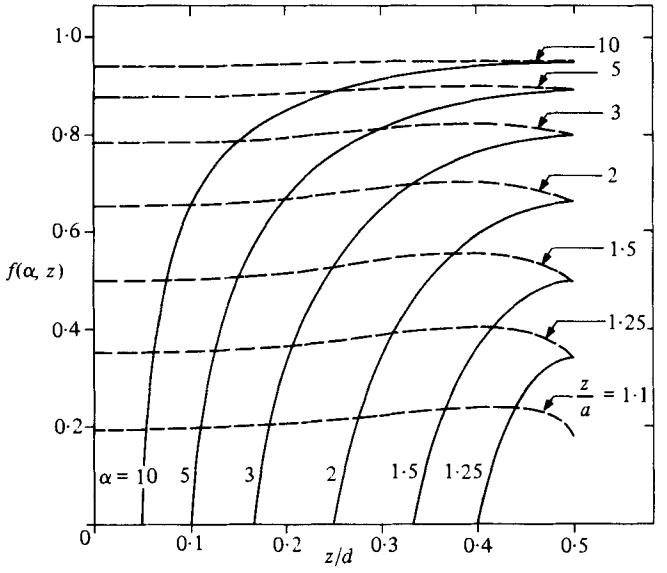

FIGURE 4. Variation of f with channel width α and particle location z/d: ——, α = const; - - - - -, z/a = const.

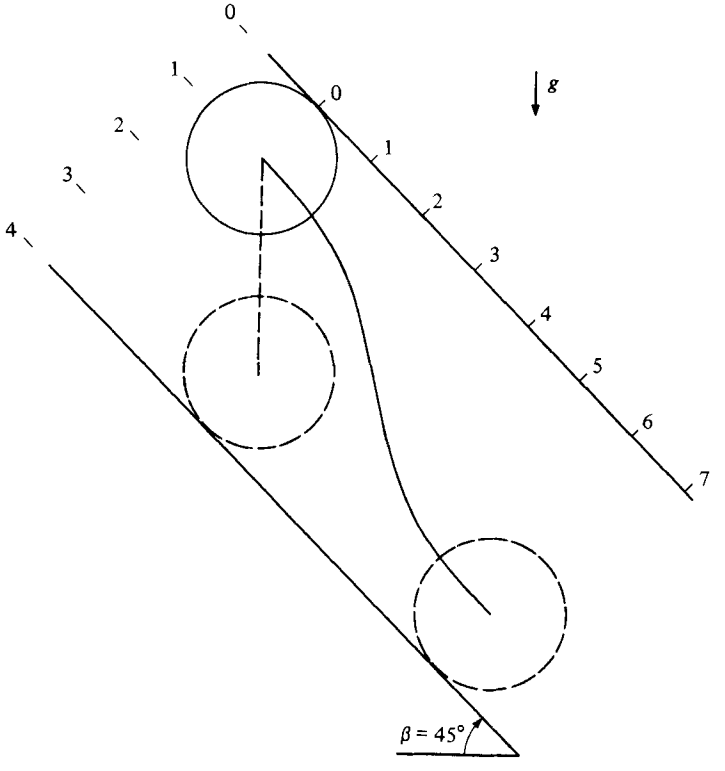

FIGURE 5. Trajectory of a sphere settling under gravity in a channel inclined at $\beta = 45°$ ($\alpha = 2$, $z_0/a = 1{\cdot}001$).

$z_0/a = 1{\cdot}001$ in a channel inclined at $\beta = 45°$ where the wall spacing is twice the sphere diameter ($\alpha = 2$). The dashed vertical line represents the trajectory that the sphere would follow in the absence of the walls. The large departure of the actual trajectory from the vertical path clearly demonstrates the strong interaction effects of the confining walls. For small gap widths the sphere moves nearly parallel to the boundary since the resistance to perpendicular motion is much larger than that to parallel motion. This behaviour is thus a consequence of the non-isotropy of the fluid resistance tensor. The trajectory is symmetric about the midplane of the channel because of the reversibility of Stokes flow.

The lateral drift of the particle can be measured by the drift angle θ shown in figure 3. For a horizontal channel ($\beta = 0$) the sphere would fall vertically, since the fluid motion is purely axisymmetric and the drift angle is zero. For a vertical channel ($\beta = 90°$) the sphere would again fall vertically, since there is no lateral force acting on the sphere in the Stokes-flow limit. This suggests that for a given channel width α and particle position z/a there is an inclination angle $\beta = \beta_{\max}$ that would give the maximum drift. To find the maximum-drift angle $\theta_{\max}$ the trigonometric relationship

$$\tan(\beta+\theta) = \frac{U_x}{U_z} \tag{3.8}$$

obtained from figure 3 is combined with (3.7) to give

$$\tan(\beta+\theta) = \frac{\tan\theta}{f(\alpha,z)}. \tag{3.9}$$

Differentiating (3.9) with respect to β while holding α and z constant and setting the derivative to zero yields

$$\tan\beta_{\max} = (f(\alpha,z))^{\frac{1}{2}}. \tag{3.10}$$

The corresponding maximum-drift angle is given by

$$\tan\theta_{\max} = \frac{1-f(\alpha,z)}{2(f(\alpha,z))^{\frac{1}{2}}}. \tag{3.11}$$

Figure 6 shows a plot of (3.10) and (3.11) as functions of $f(\alpha, z)$. The largest maximum-drift angle is found when the particle is in the vicinity of one of the walls ($f \sim 0$) and the channel is nearly horizontal. In this position the particle is travelling almost horizontally perpendicular to the direction of gravity! As the particle moves further away from the walls ($f \to 1$) the maximum possible drift angle decreases and the inclination that gives this maximum drift approaches 45°. Since $0 \leqslant f(\alpha,z) \leqslant 1$, the permissible range for $\beta_{\max}$ is $0 \leqslant \beta_{\max} \leqslant 45°$.

The angular velocity $a\Omega/U_t \sin\beta$ of the settling sphere has been computed using (3.6) as a function of particle position s for representative values of the channel-width/particle-diameter ratio α, and is shown in figure 7. Intuitively, one would expect that the sphere should roll along the closer wall. However, figure 7 shows that there is a range of particle positions where the sphere rotates in the opposite direction. As explained in Ganatos *et al.* (1980*b*) this reversal in the direction of rotation occurs because of the presence of a separated region of closed streamlines that forms near the more-distant wall, thereby inducing a small net torque in the direction opposite to what one might intuitively expect. As the sphere approaches one of the walls it tends to roll along the wall as expected, although there is slip between the sphere surface and the wall, and its angular velocity increases to a maximum and then decreases to zero in the lubrication limit. The maximum angular velocity occurs at

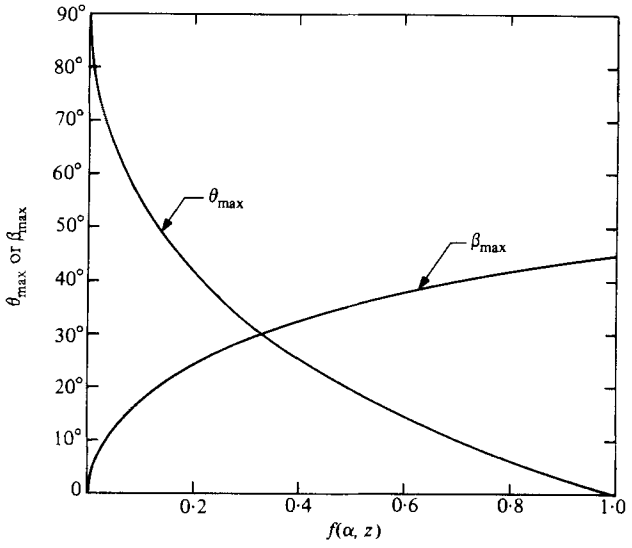

FIGURE 6. Maximum-drift angle θ_{max} and corresponding inclination angle β_{max} for a sphere settling under gravity in an inclined channel.

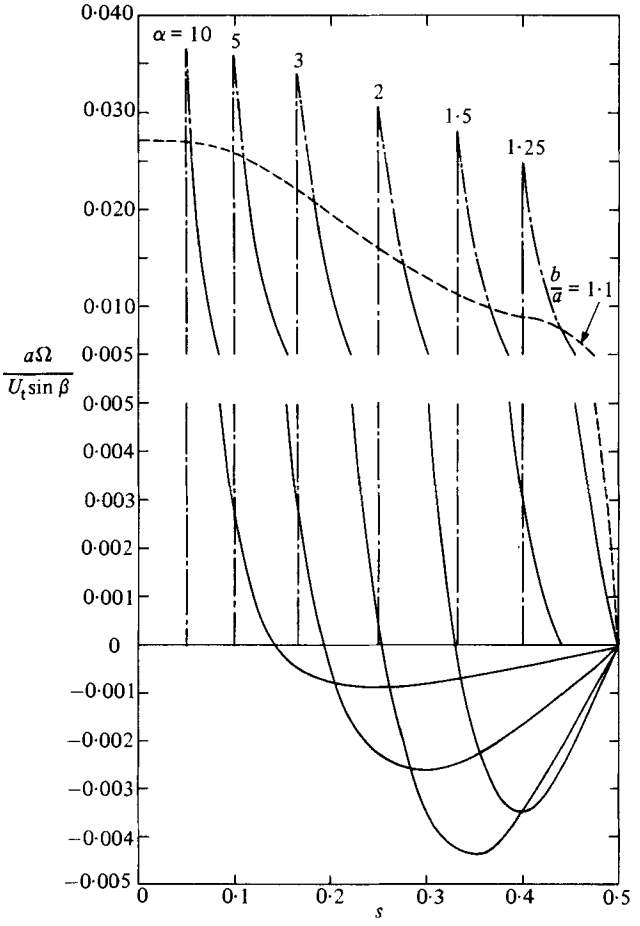

FIGURE 7. Angular velocity of a sphere settling under gravity in an inclined channel (legend as in figure 2).

a fluid gap of about 0·01 sphere radii for a channel width of 10 sphere diameters. As the channel width is decreased the maximum value of angular velocity also decreases and the maximum occurs at a particle position closer to the nearer wall. For a channel width of 1·25 diameters the maximum angular velocity occurs at a gap of about 10^{-4} sphere radii.

4. Zero-drag motion of a sphere in a channel

This section contains solutions for the motion of a neutrally buoyant sphere in Poiseuille or Couette flow in a channel. From (2.5) and (2.7) the conditions of zero force and zero torque require

$$U_x F_x^{\mathrm{t}} + a\Omega F_x^{\mathrm{r}} + V_{\mathrm{c}} F_x^{\mathrm{p}} + bS F_x^{\mathrm{s}} = 0, \tag{4.1}$$

$$U_x T_y^{\mathrm{t}} + a\Omega T_y^{\mathrm{r}} + V_{\mathrm{c}} T_y^{\mathrm{p}} + \tfrac{1}{2}aS T_y^{\mathrm{s}} = 0. \tag{4.2}$$

Note that (2.6) is not needed, since in the absence of inertia and particle deformability there is no lateral drift of the sphere relative to the planar walls. Simultaneous solution of these equations for pure two-dimensional Poiseuille flow ($S = 0$) yields

$$\frac{U_x}{V_{\mathrm{c}}} = G, \tag{4.3}$$

$$\frac{a\Omega}{V_{\mathrm{c}}} = -\frac{GT_y^{\mathrm{t}} + T_y^{\mathrm{p}}}{T_y^{\mathrm{r}}}, \tag{4.4}$$

while for simple shear flow ($V_{\mathrm{c}} = 0$)

$$\frac{U_x}{V_{\mathrm{w}}} = H, \tag{4.5}$$

$$\frac{\Omega}{\frac{1}{2}S} = -\frac{4\alpha HT_y^{\mathrm{t}} + T_y^{\mathrm{s}}}{T_y^{\mathrm{r}}}, \tag{4.6}$$

where V_{w} is the wall velocity inducing the shear flow (see figure 1). Plots of the G and H functions representing the translational velocity of the sphere as a function of channel width and particle position are shown in figures 2(b, c).

Of special interest is the local slip velocity V_{s} of the sphere centre relative to the incoming velocity profile:

$$V_{\mathrm{s}} = U_x - V_\infty. \tag{4.7}$$

For two-dimensional Poiseuille flow

$$\frac{V_{\mathrm{s}}}{V_\infty} = \frac{G}{4s(1-s)} - 1, \tag{4.8}$$

while for simple shear flow

$$\frac{V_{\mathrm{s}}}{V_\infty} = \frac{H}{s} - 1. \tag{4.9}$$

Figures 8(a, b) show a comparison of the collocation solutions for the slip velocity with the weak-interaction method-of-reflection results of Ho & Leal (1974) for Poiseuille flow and simple shear flow respectively. The weak-interaction theory gives surprisingly good results except at small particle-to-wall spacings despite large errors (mentioned in §1) in the individual force and torque coefficients comprising the G and

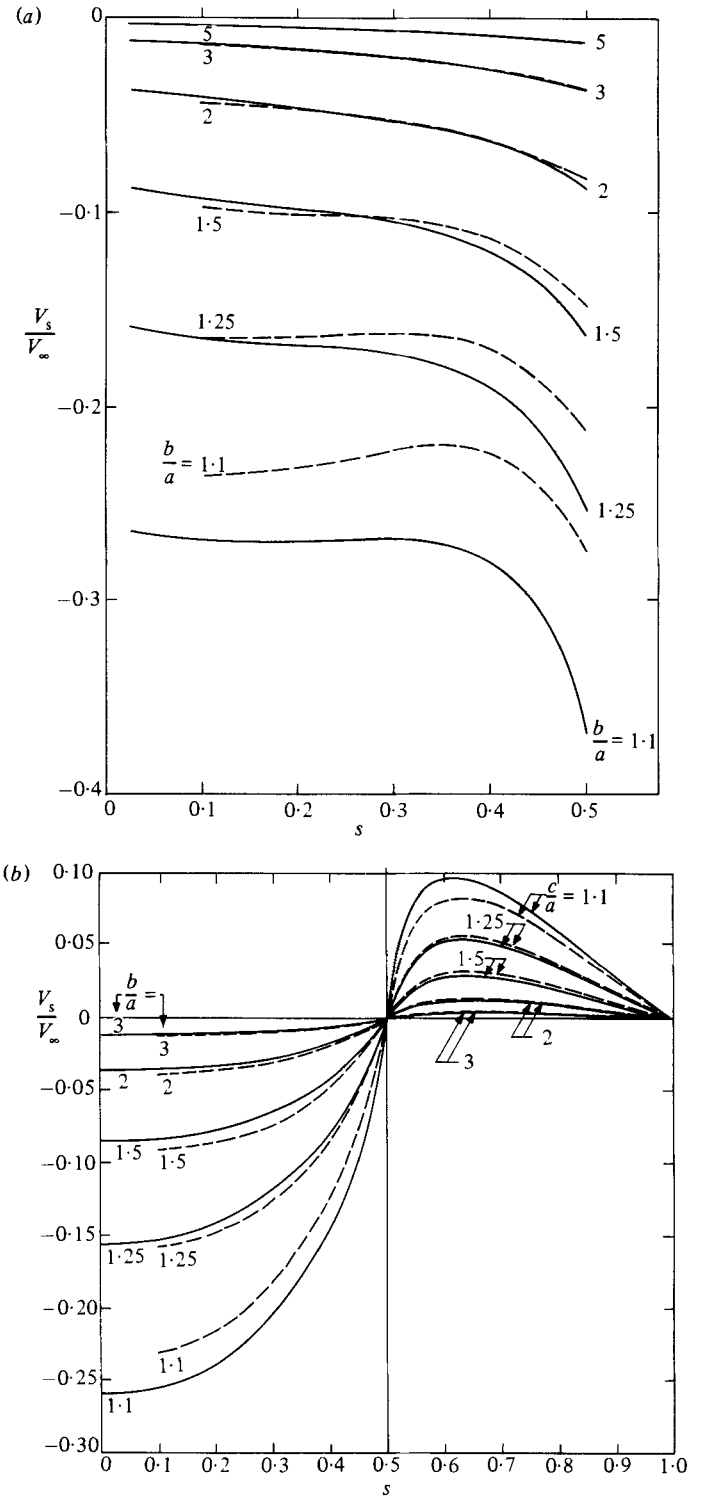

FIGURE 8. Comparison of solutions for the slip velocity of a neutrally buoyant sphere in (*a*) Poiseuille flow and (*b*) shear flow in a channel: ——, collocation theory (present study); ------, Ho & Leal (1974), weak-interaction reflection theory.

H functions (2.10), (2.11). Since the G and H functions involve ratios of the force and torque coefficients, the errors in magnitude would appear to cancel one another significantly. Nevertheless, the percentage error in the slip velocity in Poiseuille flow obtained by the weak-interaction theory can be quite high midway between the two walls where the magnitude of the slip velocity is small.

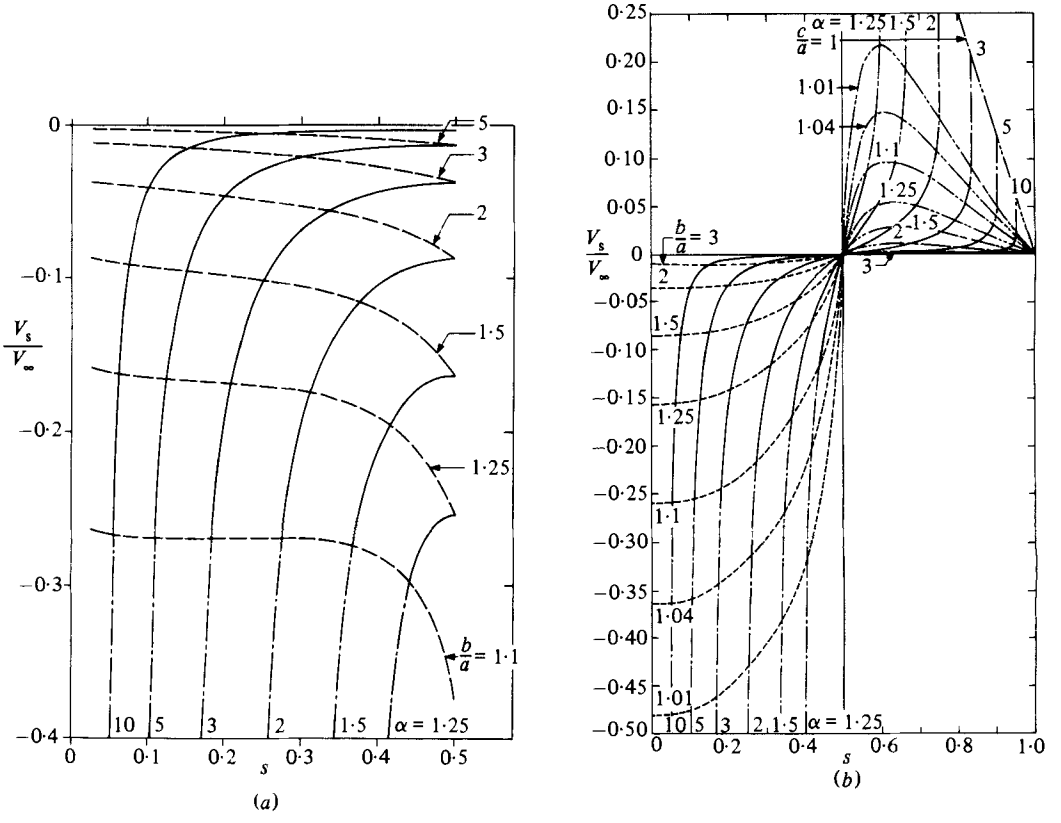

FIGURE 9. Slip velocity of a neutrally buoyant sphere in (*a*) Poiseuille flow and (*b*) shear flow in a channel: ——·——·——, c/a = const. (remaining legend as in figure 2).

Figure 9(*a*) shows the slip velocity of a neutrally buoyant sphere in Poiseuille flow as a function of wall spacing and particle position. Owing to the symmetry of the flow, the slip velocity obeys the relation

$$V_s(1-s) = V_s(s). \tag{4.10}$$

The slip velocity is negative for all values of s, indicating that the sphere lags the fluid at all positions between the two walls. For a given channel width α the sphere experiences minimum slip midway between the walls. As the sphere approaches one of the walls the G function vanishes (see figure 2*b*), and from (4.8) the ratio V_s/V_∞ approaches the value -1, indicating that the sphere sticks to the wall.

Prior to the development of the present theory it had been customary in the treatment of two phase dilute particulate systems, both in pipe and channel flow, to estimate the slip between the phases by the centreline solution for the motion of a sphere along the centreline of a circular tube, since this was the only accurate solution available. It is evident from figure 9(*a*) that the slip velocity becomes relatively much more important for particles off axis. Similarly, existing solutions

for the motion of molecules in hydrophilic membrane pores, which are also based on this centreline theory, will significantly underestimate the reflection coefficient of the membrane. This coefficient is a measure of the average slip between the phases when the statistical spatial distribution of the molecules convected by the water phase is known.

Figure 9(*b*) shows the slip velocity of a neutrally buoyant sphere in Couette flow induced by the motion of the boundary at $z = c$ (see figure 1). Here the slip velocity obeys the relation

$$V_s(1-s) = -V_s(s). \tag{4.11}$$

Thus the sphere lags the fluid for $0 \leqslant s < 0{\cdot}5$ and leads the fluid for $0{\cdot}5 < s \leqslant 1$. The slip velocity is zero midway between the two walls. As the sphere approaches the stationary wall the limiting value of the ratio V_s/V_∞ is -1. The portion of the curves $-1{\cdot}0 < V_s/V_\infty < -0{\cdot}5$ is omitted from figure 9(*b*). As the sphere approaches the moving wall the ratio V_s/V_∞ reaches the limiting value $(1-s)/s$ for $0{\cdot}5 \leqslant s \leqslant 1$, which is labelled $c/a = 1$ in figure 9(*b*). In this position the sphere is carried by the moving wall. The non-symmetry of the curves about the midplane $s = 0{\cdot}5$ is due to the non-symmetric nature of the flow field V_∞ that is used as the scaling factor.

Figure 10(*a*) shows the angular velocity of a neutrally buoyant sphere in Poiseuille flow. The angular velocity is zero midway between the walls, as expected from symmetry, and increases as the sphere approaches one of the walls. The maximum angular velocity occurs immediately adjacent to the wall, and decreases rapidly to zero in the limit as the sphere touches the wall. The maximum value of the angular velocity occurs for a channel width α slightly larger than 2 at a position where the fluid gap between the sphere and the closer wall is about 0·1 sphere radii.

Figure 10(*b*) shows similar results for the angular velocity of a neutrally buoyant sphere in Couette flow. For a fixed channel width α the angular velocity is an even function symmetric about $s = 0{\cdot}5$. As α approaches infinity the angular velocity approaches $\frac{1}{2}S$, which is the angular velocity of a neutrally buoyant sphere in an unbounded shear flow. The angular velocity is maximum at $s = 0{\cdot}5$, and monotonically approaches zero as the sphere approaches one of the walls. The portion of the figure for $2\Omega/S < 0{\cdot}65$ has been omitted.

Figure 11(*a*) shows the fluid velocity field in the plane $y = 0$ for a neutrally buoyant sphere in Couette flow located on the centreline of a channel whose width is 1·5 particle diameters. The velocity vectors shown with arrowheads have been drawn to scale and show the magnitude and direction of the fluid motion. At points in the flow field where the magnitude of the velocity is too small to be visible on the scale shown the direction of the fluid motion is shown with the aid of a straight line without an arrowhead. The Couette flow is induced by translation of the two walls with equal but opposite velocities. Since the sphere is located midway between the walls it experiences only a counterclockwise rotational motion and no translation. There are two stagnation points in the flow-field midway between the two walls fore and aft of the sphere. Between these stagnation points is a region surrounding the sphere where the fluid circulates about the sphere in closed streamlines. On the other side of these stagnation points fluid is forced across the midplane in a direction opposite to the fluid motion induced by the rotating sphere. If the walls are moved further apart the stagnation points move away from the sphere. In the absence of the walls the stagnation points are not present.

Figure 11(*b*) shows the velocity field for Poiseuille flow past a neutrally buoyant sphere for the same geometry as in figure 11(*a*). The Poiseuille flow is from right to left but is shown relative to a reference frame that is translating with the sphere, so

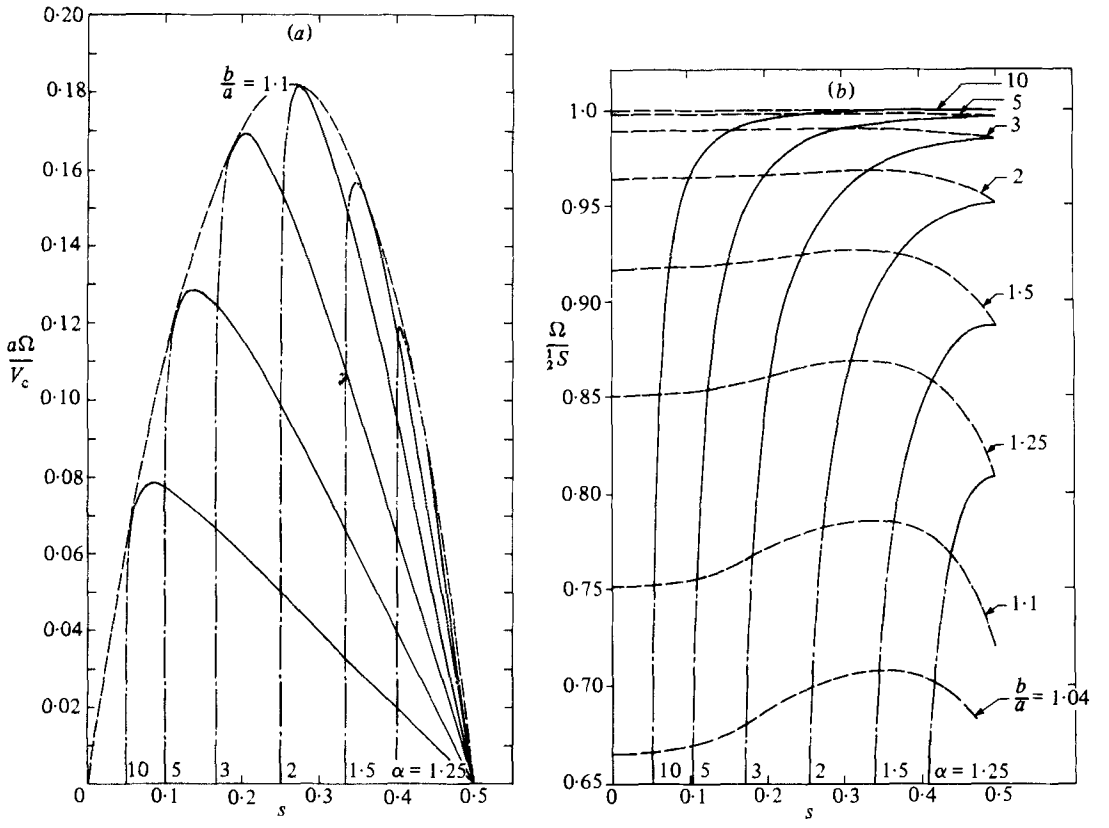

FIGURE 10. Angular velocity of a neutrally buoyant sphere in (*a*) Poiseuille flow and (*b*) shear flow in a channel (legend as in figure 2).

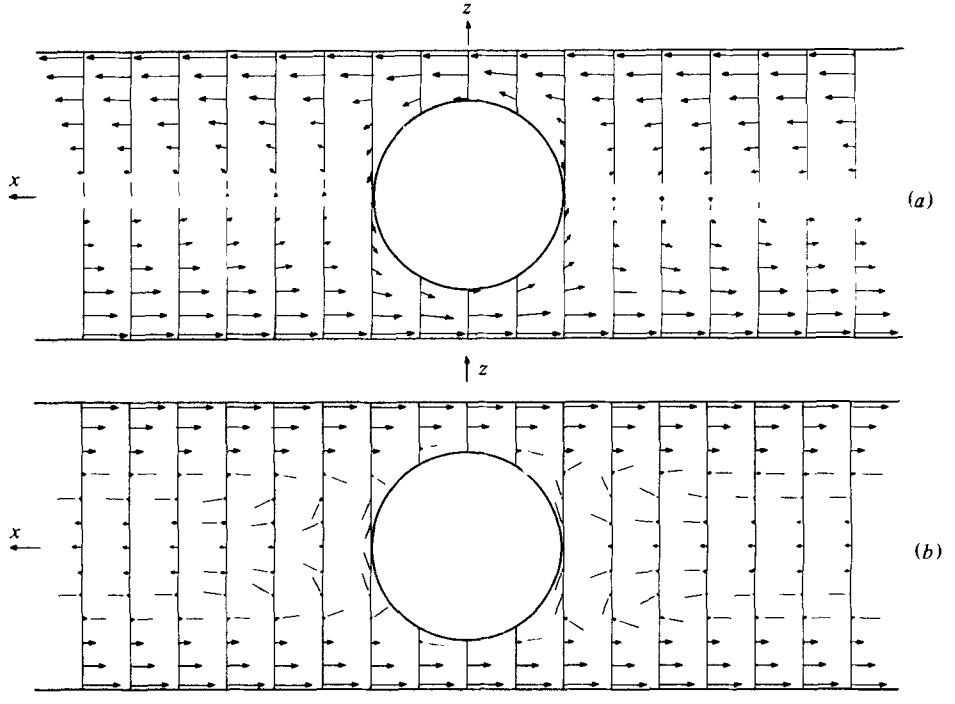

FIGURE 11. Velocity field for flow past a neutrally buoyant sphere in (*a*) shear flow and (*b*) Poiseuille flow in a channel ($\alpha = 1{\cdot}5$, $s = 0{\cdot}5$).

that the sphere appears stationary and the walls appear to be moving to the right. The angular velocity of the sphere is zero, as expected owing to the symmetry of the flow field. As can be seen in the figure, the large size of the sphere relative to the channel width causes a blockage effect, inducing circulations fore and aft of the sphere that extend to infinity. On the left side of the sphere, part of the fluid that cannot pass through the small gap between the sphere and the walls is diverted to the centre of the channel, where it is swept back by the free-stream velocity away from the sphere. On the right side of the sphere the flow pattern is reversed.

In closing, we wish to mention two related problems in low-Reynolds-number flow that are currently under investigation. One is the off-axis motion of a sphere in a circular cylinder. An exact solution of this problem is needed as input for accurate determination of the osmotic reflection coefficient and diffusion permeability in Kedem–Katchalsky membrane filtration theory for cylindrical pores. A separate paper is presently being written in which the theory for the parallel channel geometry just considered is used to determined these coefficients for pores that are two-dimensional slits between adjacent cells in a cell layer. A preliminary version of this paper has appeared as Ganatos *et al.* (1980*c*). The second problem under investigation is the tumbling motion of an ellipsoidal particle adjacent to a planar wall. The application here is to describe the motion of a red blood cell near an artery wall.

The authors wish to thank the National Science Foundation for supporting this research under grant ENG 78-22101 and the City University of New York Computer Centre for the use of their facilities.

REFERENCES

Brenner, H. 1961 *Chem. Engng Sci.* **16**, 242.

Cox, R.G. & Brenner, H. 1967 *Chem. Engng Sci.* **22**, 1753.

Dagan, Z., Weinbaum, S. & Pfeffer, R. 1982*a* *J. Fluid Mech.* **115**, 505.

Dagan, Z., Weinbaum, S. & Pfeffer, R. 1982*b* *J. Fluid Mech.* **117**, 143.

Faxen, H. 1923 *Ark. Mat. Astron. Fys.* **17**, no. 27.

Ganatos, P. 1979 Ph.D. dissertation, City University of New York.

Ganatos, P., Pfeffer, R. & Weinbaum, S. 1978 *J. Fluid Mech.* **84**, 79.

Ganatos, P., Pfeffer, R. & Weinbaum, S. 1980*b* *J. Fluid Mech.* **99**, 755.

Ganatos, P., Weinbaum, S., Fischbarg, J. & Liebovitch, L. 1980*c* In *Advances in Bioengineering*, p. 193. A.S.M.E.

Ganatos, P., Weinbaum, S. & Pfeffer, R. 1980*a* *J. Fluid Mech.* **99**, 793.

Gluckman, M. J., Pfeffer, R. & Weinbaum, S. 1971 *J. Fluid Mech.* **50**, 705.

Goldman, A. J., Cox, R. G. & Brenner, H. 1967*a* *Chem. Engng Sci.* **22**, 637.

Goldman, A. J., Cox, R. G. & Brenner, H. 1967*b* *Chem. Engng Sci.* **22**, 653.

Ho, B. P. & Leal, L. G. 1974 *J. Fluid Mech.* **65**, 365.

Leichtberg, S., Pfeffer, R. & Weinbaum, S. 1976 *Int. J. Multiphase Flow* **3**, 147.

Wang, H. & Skalak, R. 1969 *J. Fluid Mech.* **38**, 75.